

## 11 - INTERSTELLAR DUST

### *General Processes*

Extinction

Reddening ( $\lambda$ -selective extinction)

Scattering (reflection nebulae)

Thermal IR Emission

Polarization (by scattering & selective extinction)

### *Re-Introduction to MAGNITUDES*

$$m(\lambda) = -2.5 \log \mathfrak{S}_\lambda + \text{const.}(\lambda)$$

$$m_{*2}(\lambda) - m_{*1}(\lambda) = 2.5 \log \left\{ \frac{\mathfrak{S}_{*1}(\lambda)}{\mathfrak{S}_{*2}(\lambda)} \right\} \quad \text{two stars at one wavelength}$$

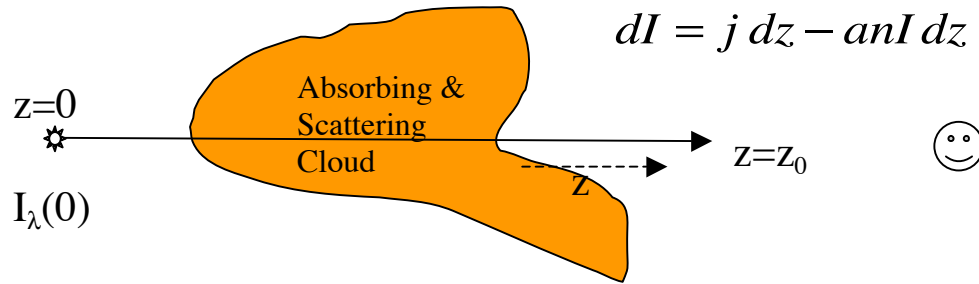
$$m_{\lambda_2} - m_{\lambda_1} = 2.5 \log \left\{ \frac{\mathfrak{S}_{\lambda_1}}{\mathfrak{S}_{\lambda_2}} \right\} - \text{const.} \quad \text{one star at two wavelengths}$$

“Alphabet Soup Photometry”

UBVRIJHKLMNQ.....

$$"B - V" = m_B - m_V = 2.5 \log \left\{ \frac{\mathfrak{S}_V}{\mathfrak{S}_B} \right\} - \text{const.}$$

Extinction = Absorption + Scattering



$$\frac{dI_\lambda}{dz} = j_\lambda - a_\lambda n I_\lambda = -a_\lambda n I_\lambda \quad \text{if } j_\lambda = 0$$

$$\text{let } d\tau_\lambda \equiv a_\lambda n dz \quad \tau_\lambda = \int_{z=0}^{z=z_0} a_\lambda n dz$$

$$\frac{dI_\lambda}{I_\lambda} = -d\tau_\lambda \quad \ln I_\lambda = -\tau_\lambda + \text{const.}$$

$$\text{for } \tau_\lambda = 0 \quad \ln I_\lambda = \ln I_\lambda(0)$$

$$I_\lambda(\tau_\lambda) = I_\lambda(0) e^{-\tau_\lambda}$$

$$A_\lambda(\text{mags}) = 2.5 \log \frac{I_\lambda(0)}{I_\lambda(\tau_\lambda)} = 2.5 \log(e^{\tau_\lambda})$$

$$= 2.5 \tau_\lambda \underbrace{\log e}_{0.4343\dots}$$

$$A_\lambda = 1.086 \tau_\lambda$$



Color Excess  $E(\lambda_2 - \lambda_1) = A(\lambda_2) - A(\lambda_1) = [m_{\lambda_2}(\tau_{\lambda_2}) - m_{\lambda_2}(0)] - [m_{\lambda_1}(\tau_{\lambda_1}) - m_{\lambda_1}(0)]$

$$E(\lambda_2 - \lambda_1) = [m_{\lambda_2}(\tau_{\lambda_2}) - m_{\lambda_1}(\tau_{\lambda_1})] - [m_{\lambda_2}(0) - m_{\lambda_1}(0)]$$

*i.e.*  $E(B-V) = (B-V)_{\text{observed}} - (B-V)_{\text{true}}$

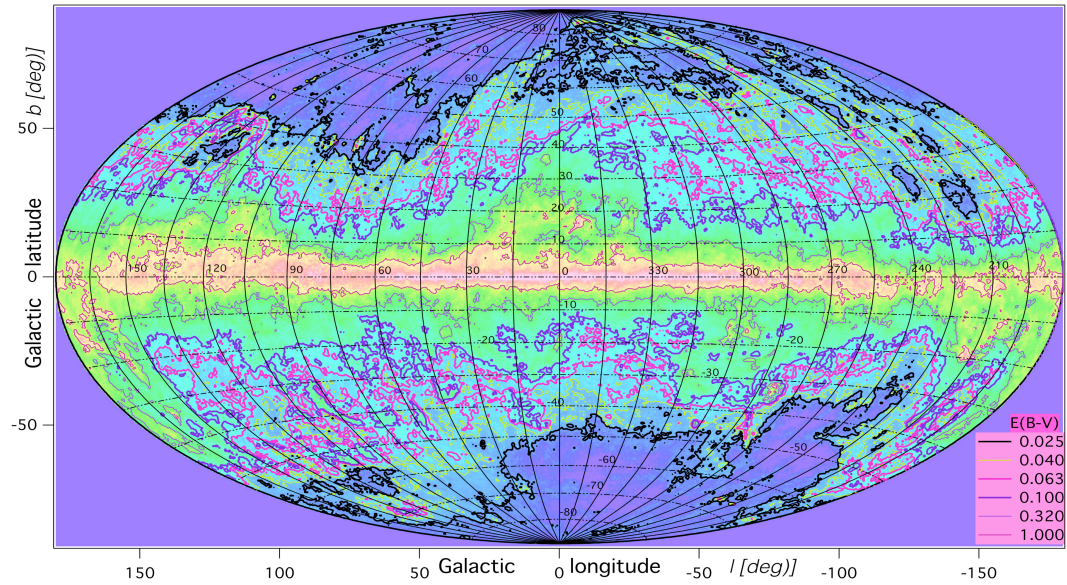


**Figure 8.** The Schlegel et al (1998) dust map is reproduced, along with the traces of the vertical planes of Fig 4 to 7 superimposed. The color-coded quantity is the logarithm of  $E(B-V)$ . The six contours are for  $\log(E(B-V))=0$  (thin pink),  $-0.5$  (thin violet),  $-1$  (thick violet),  $-1.2$  (thick pink),  $-1.4$  (yellow) and  $-1.6$  (black). Counterparts to the tenuous clouds at mid or high latitudes that appear in this SFD map can be searched for in Fig 4 to 7, using the  $l, b$  grid.

Map of  $E(B-V)$  from Lallement et al. arXiv:1309.6100 (reproduced from Schlegel et al 1998, ApJ, 500, 525)

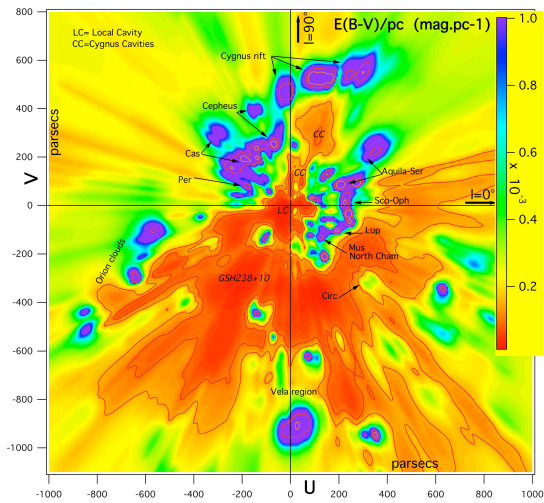


**Figure 1.** The inverted differential opacity distribution in the Galactic Plane. The Sun is at coordinates  $(x,y)=(0,0)$  and the Galactic center direction at right. The opacity increases from red to violet (scale at right). Note the 1,000 pc long cavity centered at  $l \approx +225^\circ$  that we identified as the major super-bubble GSH238+00+09 detected in radio by Heiles(1998). We have called *Cygnus cavities* the empty regions at  $l \approx +70^\circ$ . Several well known opaque regions are indicated on the maps, their identification is based on the literature. The gradient axis for interstellar Helium ionization point to the center of the GSH238+00+09.

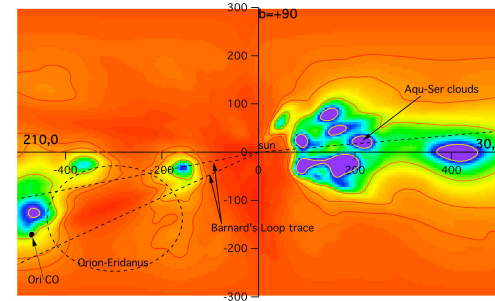
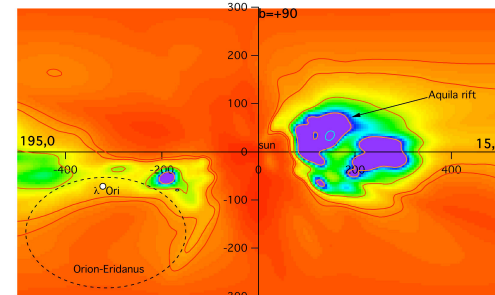
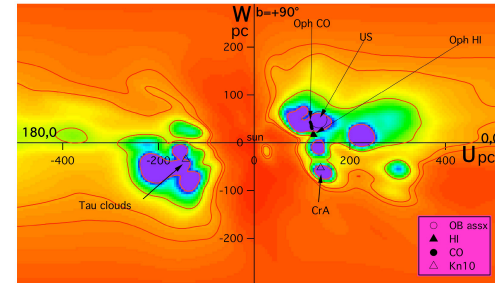


**Figure 4.** Opacity distribution in vertical planes containing the Sun, equally spaced by  $15^\circ$ . The North pole direction  $b=+90^\circ$  is at top and longitudes of intersections with the Galactic Plane are indicated. Some iso-differential opacity contours have been superimposed to help visualizing the low and high opacity regions. OB associations from De Zeeuw (1999) as well as CO and HI clouds listed by Perrot & Grenier(2003) have been displayed when they are within 25 pc from this vertical plane. We also add the molecular cloud locations derived by Knude(2010). Note the tenuous cloud close to the North Pole direction.

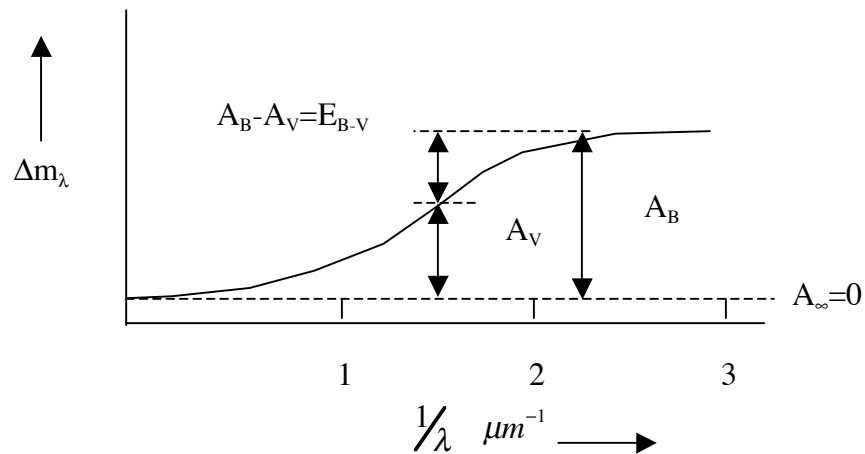
Figures from Lallement et al. arXiv:1309.6100

*Total-to-Selective Extinction* – traditionally done in B and V:

$$R_V \equiv \frac{A_V}{E(B-V)} = \frac{A_V}{A_B - A_V} = \frac{a_V}{a_B - a_V}$$

*Pair Method to get  $A_\lambda$  and  $R$*

Compare 2 stars (ratio of their fluxes) of the same intrinsic color (same  $T_{\text{surf}}$  or B-V)



Results – usually  $R \sim 3-3.5$ , with  $\langle R \rangle \sim 3.1$

To compare extinction curves of stars with different amounts of dust along the line of sight, it will be necessary to normalize them in some fashion. Usually this is done by dividing by the  $E(B-V)$  for each star.

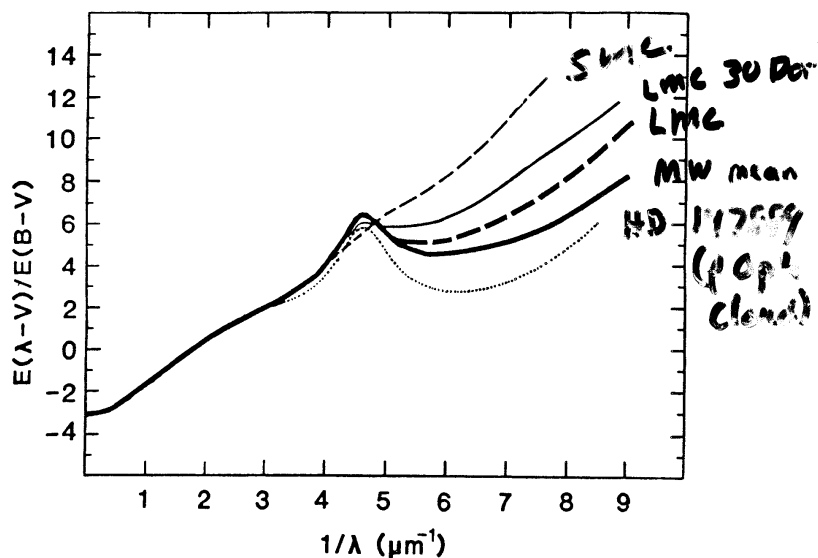
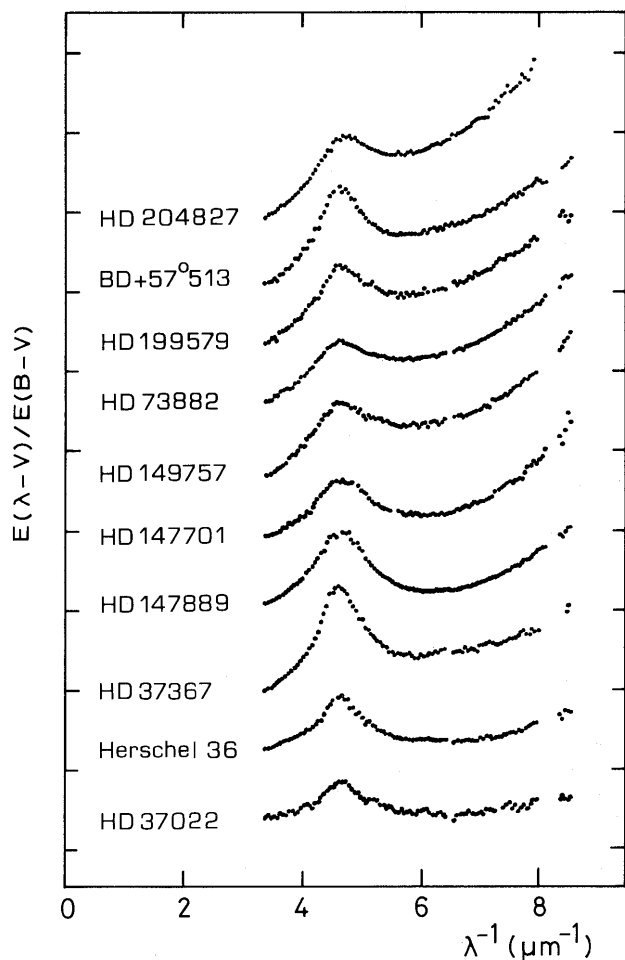


Fig. 1. Several extinction laws, all normalized to a difference of unity between the  $V$  and  $B$  filters, plotted against wave number. Heavy solid line: the average curve in the diffuse regions of the Milky Way galaxy. Heavy dashed: the average in the Large Magellanic Cloud outside of the 30 Doradus region (Fitzpatrick 1985). Light solid: Average for stars in the 30 Doradus region of the Large Magellanic Cloud. Light dashed: the extinction in the Small Magellanic Cloud (Prevot *et al.*, 1984). Dotted: HD 147889, a B star within the  $\rho$  Ophiuchus dark cloud, emphasizing that dust in dark clouds is not the same as that in diffuse regions.

All of the curves are characterized by an overall increase in extinction with decreasing wavelength, with a slight “shoulder” in the visible, and a distinct peak in the UV near 2175 Å. This feature is an indicator of carbonaceous material.

Table 3.1 The average extinction curve with  $B, V$  normalization.

$\lambda$ ( $\mu\text{m}$ )	$\lambda^{-1}$ ( $\mu\text{m}^{-1}$ )	$E_{\lambda-V}/E_{B-V}$	$A_{\lambda}/A_V$
$\infty$	0	-3.05	0
4.8	0.21	-2.98	0.02
3.5	0.29	-2.93	0.04
2.22	0.45	-2.77	0.09
1.65	0.61	-2.58	0.15
1.25	0.80	-2.25	0.26
0.90	1.11	-1.60	0.48
0.70	1.43	-0.78	0.74
0.55	1.82	0.00	1.00
0.44	2.27	1.00	1.33
0.40	2.50	1.30	1.43
0.344	2.91	1.80	1.59
0.274	3.65	3.10	2.02
0.25	4.00	4.19	2.37
0.24	4.17	4.90	2.61
0.23	4.35	5.77	2.89
0.219	4.57	6.57	3.15
0.21	4.76	6.23	3.04
0.20	5.00	5.52	2.81
0.19	5.26	4.90	2.61
0.18	5.56	4.65	2.52
0.17	5.88	4.77	2.56
0.16	6.25	4.85	2.59
0.149	6.71	5.05	2.66
0.139	7.18	5.39	2.77
0.125	8.00	6.55	3.15
0.118	8.50	7.45	3.44
0.111	9.00	8.45	3.77
0.105	9.50	9.80	4.21
0.100	10.00	11.30	4.70



**Figure 3.6** Comparison of the ultraviolet extinction curves of 10 stars observed with IUE (Fitzpatrick and Massa 1986, 1988). The vertical axis is  $E_{\lambda-V}/E_{B-V}$  (one division = 4 magnitudes), individual curves being displaced vertically for display.

There are variations in the extinction law, especially evident at UV wavelengths. These have been parameterized by Cardelli, Clayton, and Mathis (1989, ApJ, 345, 245):

$$\frac{E_{\lambda-V}}{E_{B-V}} = \underbrace{(c_1 + c_2 x)}_{\text{linear term}} + \underbrace{c_3 D(x)}_{\text{bump term}} + \underbrace{c_4 F(x)}_{\text{far-UV rise}} \quad \text{where } x = \lambda^{-1}$$

What do these extinction curves tell us about the nature of the grains?

## Optical Properties of Small Particles

individual spherical grain:  $\sigma_{\substack{\text{Extinction} \\ \text{Absorption} \\ \text{Scattering}}} = \underbrace{\pi a^2}_{\text{geometric cross-section}} \underbrace{Q_E}_{\substack{A \\ S \\ \text{efficiency} \\ \text{factor}}} \text{ cm}^2/\text{particle}$  AND net  $\left\{ \begin{array}{l} \text{Extinction} \\ \text{Absorption} \\ \text{Scattering} \end{array} \right\}$  coeff.  $C(\lambda) = \int_0^\infty n(a) \pi a^2 Q(a, \lambda) da$

Define  $x \equiv \frac{2\pi a}{\lambda}$  and let the complex index of refraction be  $m = n + ik$

### 2 Basic Limits:

<p>A. <math>x \ll 1</math> Rayleigh Limit</p> $Q_{abs} = 4x \operatorname{Im} \left\{ \frac{m^2 - 1}{m^2 + 2} \right\}$ $Q_{scat} = \frac{3}{8} x^4 \left  \frac{m^2 - 1}{m^2 + 2} \right ^2$ $Q_{ext} = Q_{abs} + Q_{scat}$ <p>When <math>k \neq 0</math>, if <math>x \ll 1</math>, then <math>Q_{scat} \sim 0</math> and <math>Q_{ext} \sim Q_{abs}</math>.</p>	<p>B. <math>x \gg 1</math> ("Brick" limit) but still in diffraction limit</p> $Q_{ext} \rightarrow 2 \quad (!!)$ <p>Look at the extinction curve in the Ch. 5 notes!</p>	
---	--	--

What is  $n(a)$ ? Seems to be  $n(a) \sim a^{-3.5}$ , with a maximum and minimum size limit. What is the total  $n_{\text{dust}}$ ? Let us make an educated guess:

Let  $x \sim 2$ ,  $\lambda \sim 0.5 \mu\text{m}$ ,  $Q_{\text{ext}} \sim 2$

$$\sigma_{\lambda} \sim \frac{5}{\pi} \times 10^{-9} \text{ cm}^2 / \text{particle} \text{ and } \tau_{\lambda} = n_{\text{dust}} \sigma_{\lambda} \underbrace{s}_{\substack{\text{path} \\ \text{length}}} = \frac{A_{\lambda}}{1.086}$$

$$\therefore n_{\text{dust}} = \frac{A_{\lambda}}{1.086 \sigma_{\lambda} s}$$

$$\text{OBSERVATION } \frac{A_{\lambda}}{s} \sim 1 \text{ mag kpc}^{-1} \text{ so } \frac{A_{\lambda}}{s} \sim \frac{1}{3 \times 10^{21} \text{ cm}} \Rightarrow n_{\text{dust}} \sim 2 \times 10^{-13} \text{ cm}^{-3}$$

What is the MASS DENSITY of dust in the interstellar medium?

$$\text{mass density} = n_{\text{dust}} \underbrace{\frac{4}{3} \pi a_{\text{dust}}^3 \rho_{\text{dust}}}_{\text{mass per grain}}$$

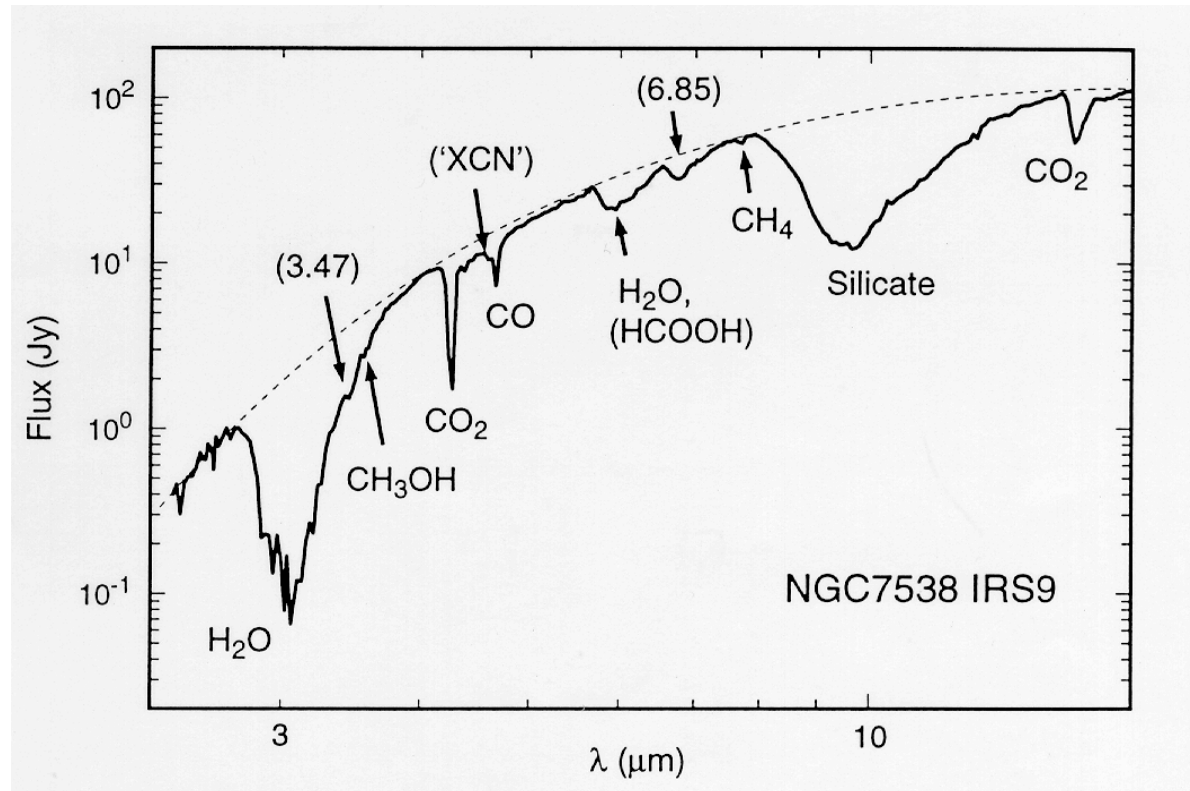
$$\rho_{\text{dust}} \sim 3 \text{ g cm}^{-3} \Rightarrow \text{mass density (dust)} \sim 10^{-26} \text{ g cm}^{-3}$$

$$n_{\text{gas}} \sim 0.5 \text{ cm}^{-3} \Rightarrow \text{mass density (gas)} \sim 10^{-24} \text{ g cm}^{-3}$$

$$\frac{\text{mass of dust}}{\text{mass of gas}} \sim 10^{-2}$$

Because of this, astronomers often refer to the “gas-to-dust ratio” being  $\sim 100$ .

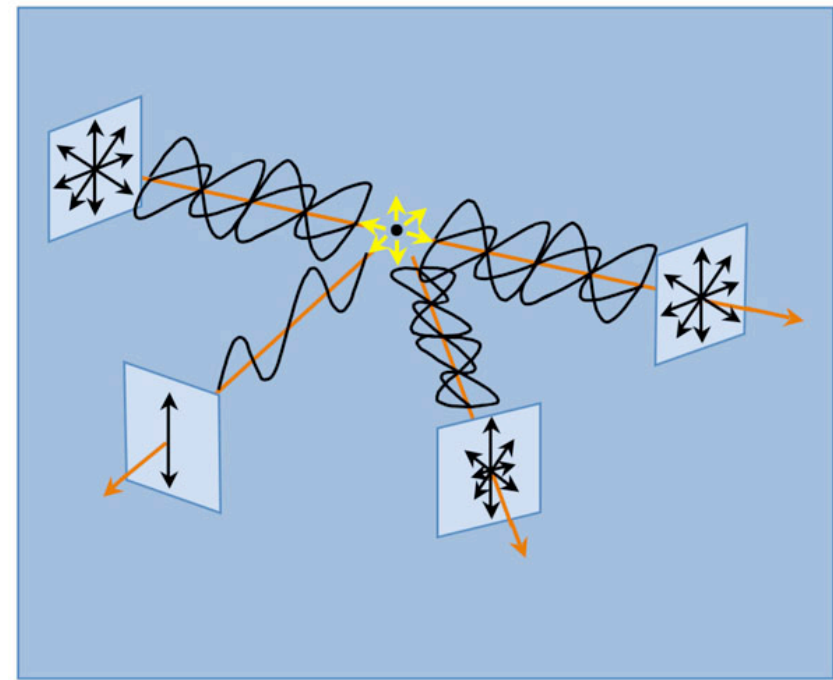
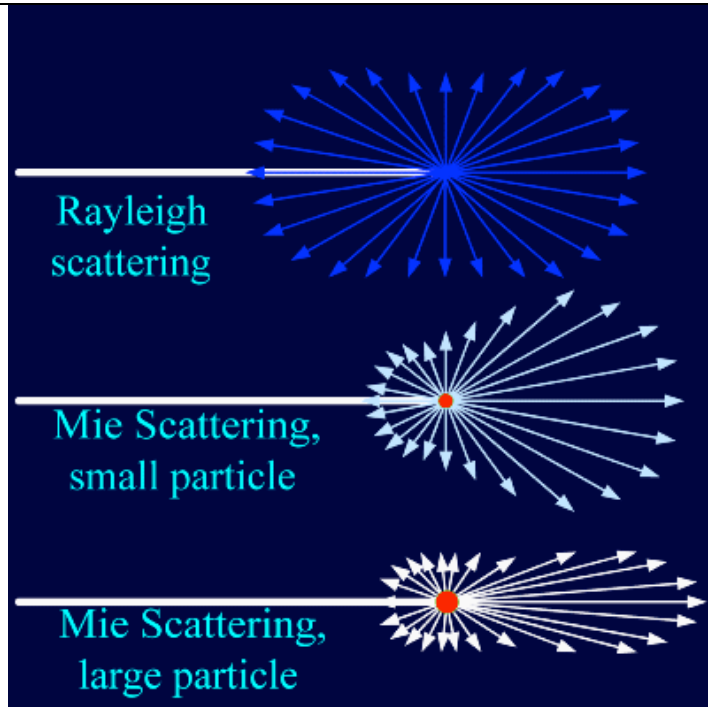
Now, looking at longer wavelengths, we see additional features. Some of these are due to ices, and are found only in cold dark clouds. A strong silicate absorption band is seen in both cold molecular clouds and warmer diffuse clouds.



As we will see later, traditionally the observed extinction curves have been modeled as a mixture of silicate particles and carbonaceous particles, specifically graphite.



## POLARIZATION



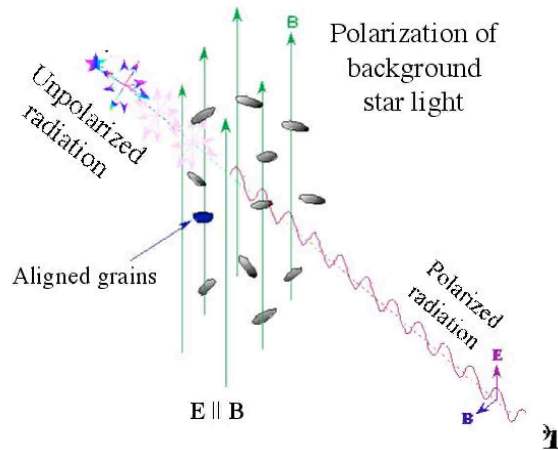
When light scatters off of small particles, the *scattering phase function* will depend on the relative size of the particles to the wavelength of the light - i.e. the previously-mentioned size parameter  $X = \frac{2\pi \cdot \text{radius}}{\text{wavelength}}$ .

Polarization will also occur when light is scattered off of small particles. In this case we are considering only linear polarization. If one passes the light through a “perfect” polarizing filter, the fractional polarization is determined from the maximum and minimum intensity observed:

$$P = \frac{I_{\max} - I_{\min}}{I_{\max} + I_{\min}}$$

But interstellar grains can act as polarizing filters also!

Polarization due to aligned grains:



We see the maximum polarization when looking  $\perp$  to the direction of the magnetic field lines, and zero when looking  $\parallel$  to it. Figure from Lazarian arXiv:0811.1020.

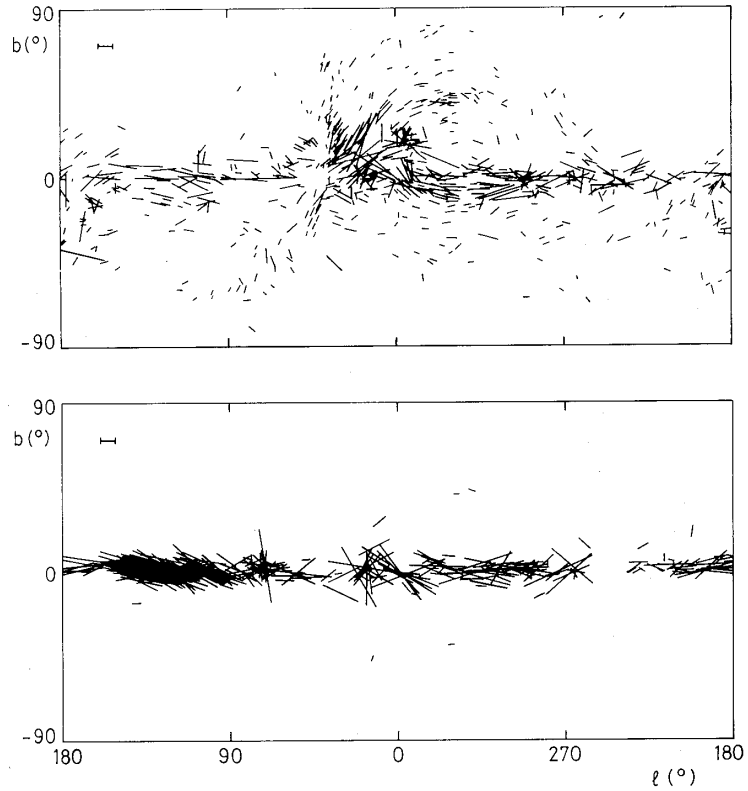
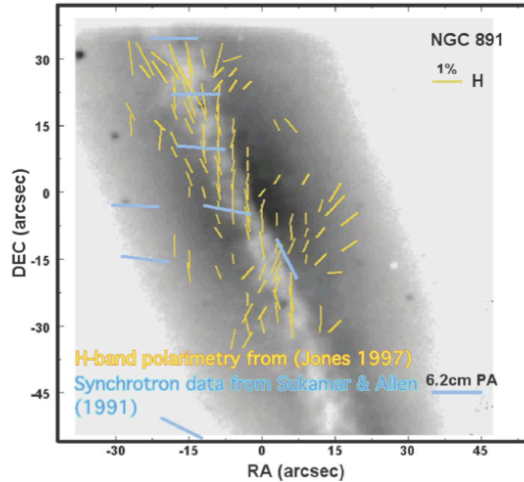
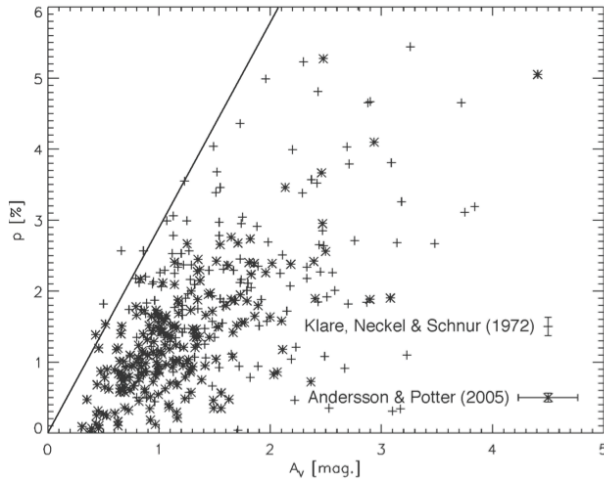


Figure 4.3 Distribution of polarization vectors in galactic coordinates  $(\ell, b)$ , based on data from the catalogue of Axon and Ellis (1976). Upper frame: nearby stars ( $d < 400$  pc), illustrating structure in the magnetic field associated with local clouds. Lower frame: stars in the distance interval  $2 < d < 4$  kpc, illustrating the effect of alignment averaged over many clouds. The length of the bar at top left in each frame indicates 1% polarization. Only stars with  $P_V > 0.2\%$  are plotted.



The polarization has an upper limit of  $\frac{P}{A_v} \sim 3.0\% \text{ mag}^{-1}$  representing optimum grain alignment. The plane of polarization, when compared to that of synchrotron radiation in other galaxies, is consistent with grains aligned normal to the magnetic field direction. (From B.-G. Anderson (2012)).

The polarization is a function of the wavelength. The total polarization to a star will depend on both the amount of dust along the line of sight, as well as the degree of grain alignment. All stars exhibit a maximum in their polarizations in the visible wavelength region, but the exact value of  $\lambda_{\text{max}}$  varies from object to object, and seems to correlate with R.

Nevertheless, there seems to be a “universal” polarization curve when normalized to  $P_{\text{max}}$  and  $\lambda_{\text{max}}$ :

$\frac{P_\lambda}{P_{\text{max}}} = \exp\left\{-K \ln^2\left(\frac{\lambda_{\text{max}}}{\lambda}\right)\right\}$  with  $K=1.15$ . The parameter K determines the width of the curve. This relationship is referred to as Serkowski’s Law. Somewhat better fits to stars are obtained by letting K vary somewhat. Fits to the actual data suggest that K depends on the value of  $\lambda_{\text{max}}$  ( $K=c_1\lambda_{\text{max}}+c_2$ : Wilking’s Law).

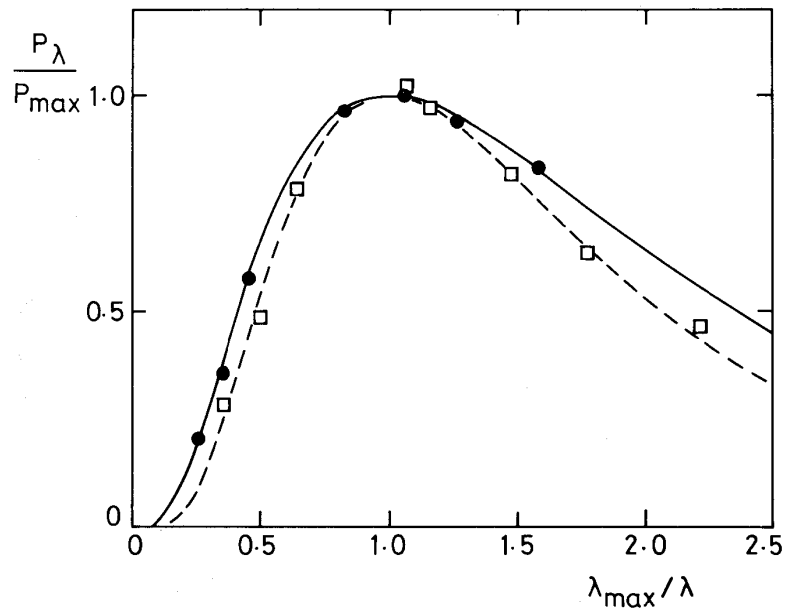
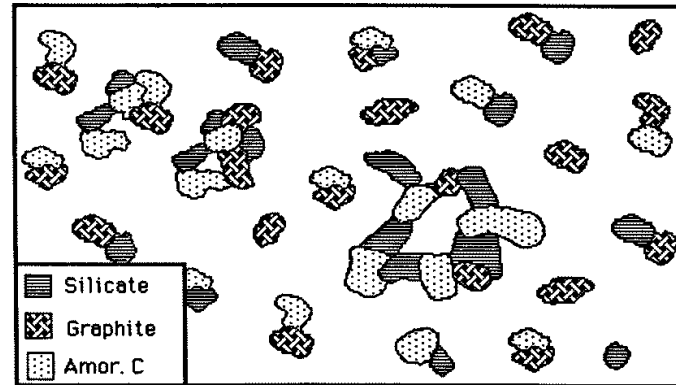


Figure 4.6 Normalized interstellar linear polarization curves for two stars with contrasting values of  $\lambda_{\max}$ . Observational data (points) are compared with empirical fits based on the Wilking law for HD 42087 ( $\lambda_{\max} = 0.57 \mu\text{m}$ , filled circles and continuous curve), and HD 147889, ( $\lambda_{\max} = 0.80 \mu\text{m}$ , open squares and dashed curve). Data are from Wilking *et al* (1980) and references therein.

To produce the observed polarizations, modelers invoke elongated silicate grains that are aligned with the galactic magnetic field. There are many models. One “obvious” one is by ferromagnetic inclusions.



Grain Albedos  $\text{albedo } \varpi = \frac{C_{scat}}{C_{ext}}$

This can *in principle* be determined by observing reflection nebulae and the *diffuse galactic light*.

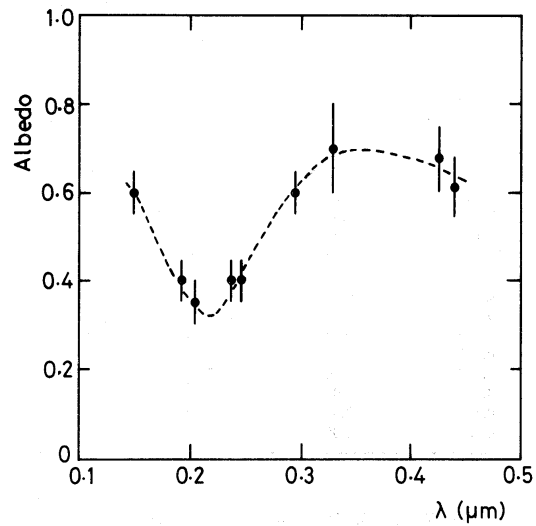
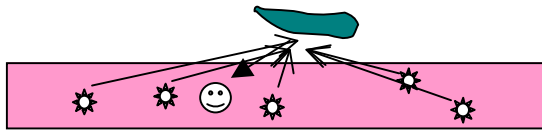


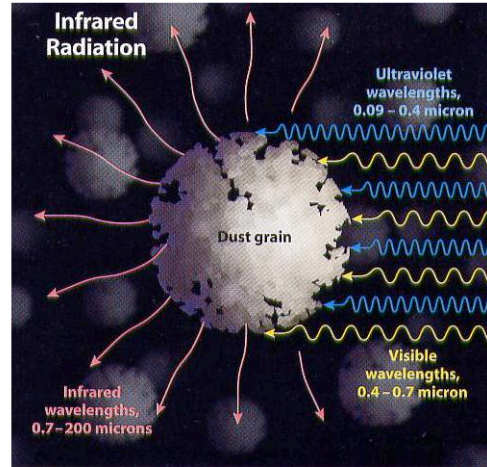
Figure 3.4 The spectral dependence of the albedo from 0.1 to 0.5  $\mu\text{m}$ , deduced from observations of the diffuse galactic light (Lillie and Witt 1976; Toller 1981).

It appears as if the 2175  $\text{\AA}$  feature seen in the interstellar extinction curve is an *absorption* feature. However, these sorts of calculations are very uncertain.

## Heating of Grains by Stars

$$E_{in} = \int_{UV} 4\pi J_{v*} \pi a^2 Q_{abs}(a, \lambda) d\nu$$

$$E_{out} = \int_{IR} 4\pi a^2 \pi B_{\nu}(T_{grain}) Q_{abs}(a, \nu) d\nu$$



Typically,  $Q_{abs, UV} \sim 1$   $Q_{abs, IR} \sim q\nu^{\gamma}$  where  $\gamma \sim 1.6$

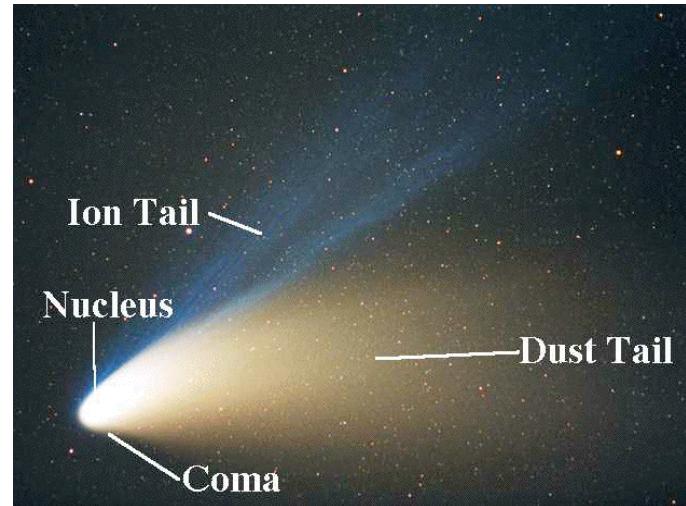
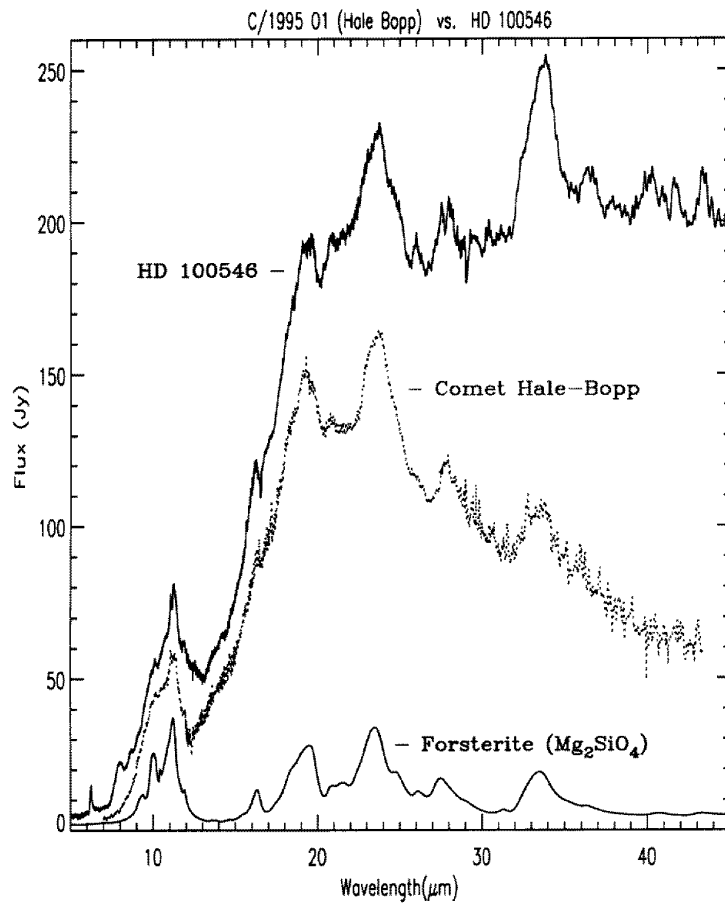
In equilibrium, 
$$T_g = \frac{h}{k} \left[ \frac{1}{q_{IR}} \frac{L_*}{4\pi r^2} \frac{c^2}{8\pi h} \frac{1}{\Gamma(4+\gamma)\zeta(4+\gamma)} \right]^{1/4+\gamma}$$

Using  $\gamma \sim 1.6$  and  $q \sim 1.4 \times 10^{-24}$ , 
$$T_g \sim 10 \left[ \frac{L_* / L_{\odot}}{r_{pc}^2} \right]^{1/5.6} e^{-\tau_{uv}/5.6} \left[ \frac{0.05}{a_{\mu m}} \right]^{1/5.6}$$

For  $L \sim 10^6 L_{\odot}$ ,  $r=1$  pc,  $\tau=0$  this gives  $T_g \sim 120$  K (peak emission at  $\sim 24 \mu m$ ) in  $F_{\lambda}$  units.

## WHAT ARE THE GRAINS?

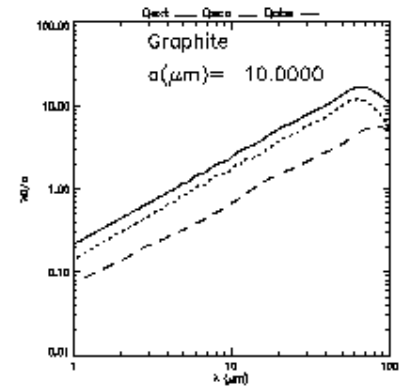
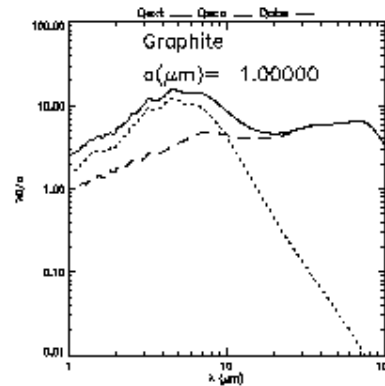
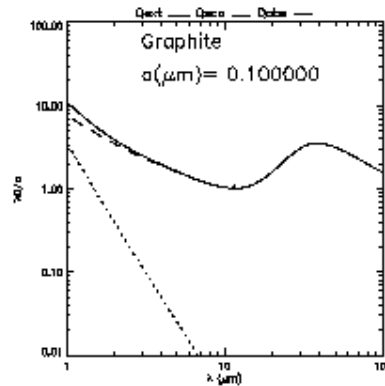
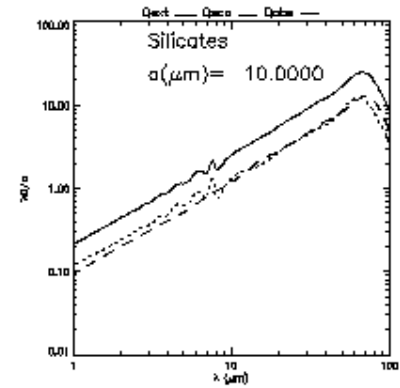
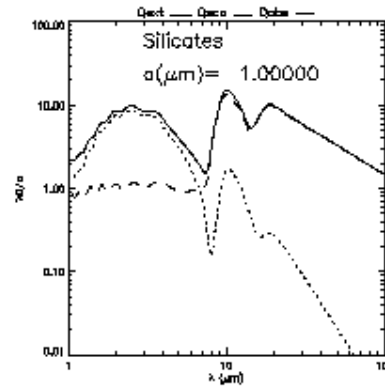
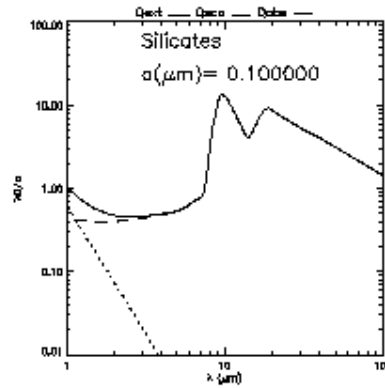
**Silicates** – main bands near 9.7  $\mu\text{m}$  (SiO stretch), 20  $\mu\text{m}$  (SiO bend) + many others at longer wavelengths. Seen in absorption in the ISM, emission and absorption for dust surrounding stars.



*IR spectra of the dust surrounding the Herbig Ae/Be star HD 100546, Comet Hale-Bopp, and laboratory sample of forsterite (Mg-rich olivine silicate).*

**Carbon Stuff:** all C-rich materials absorb near 0.22  $\mu\text{m}$ . Graphite has been a favorite because its optical constants was measured in the laboratory decades ago. Diamonds are another component – nanodiamonds are found in meteorites, for example. But the actual C-stuff may be a complex mess, since C forms so many complex molecules. More on these later...

Because silicates and carbonaceous material dominate the spectral features seen in the diffuse clouds, the interstellar extinction curve has traditionally been modeled (with some success) as a mixture of silicate grains and graphite grains. Usually Mie theory is used.





The “classic” paper outlining a fit to the overall extinction curve is that of Mathis, Rumpl, and Nordseick (1977 ApJ, 217, 425), who used just this mixture, an  $n(a) \sim a^{-3.5}$  size distribution, and a size range of  $0.005 \mu\text{m} - 1 \mu\text{m}$  (later revised to  $0.25 \mu\text{m}$ ). This mix is commonly referred to as the “MRN” mix.

J. Mayo Greenberg developed an alternate model, based on his studies of the processing of icy mantles on silicate grains under conditions simulating those in cold molecular clouds. There, cosmic rays will convert these ices into an organic refractory material (“yellow stuff”) to produce a core-mantle structure.

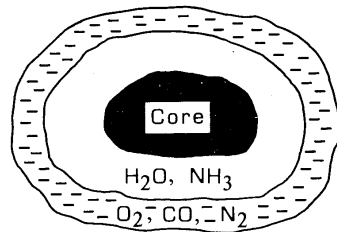


Figure 7.11 A schematic representation of grain structure in a dense molecular cloud. The core is composed of refractory materials such as silicates, amorphous carbon and organic residues. The inner mantle is composed largely of polar molecules which form by surface reactions in the presence of H I, and is dominated by H<sub>2</sub>O. The outer mantle is composed predominantly of non-polar molecules such as O<sub>2</sub>, N<sub>2</sub> and CO, which form in an H<sub>2</sub> environment.

Other models exist as well.....

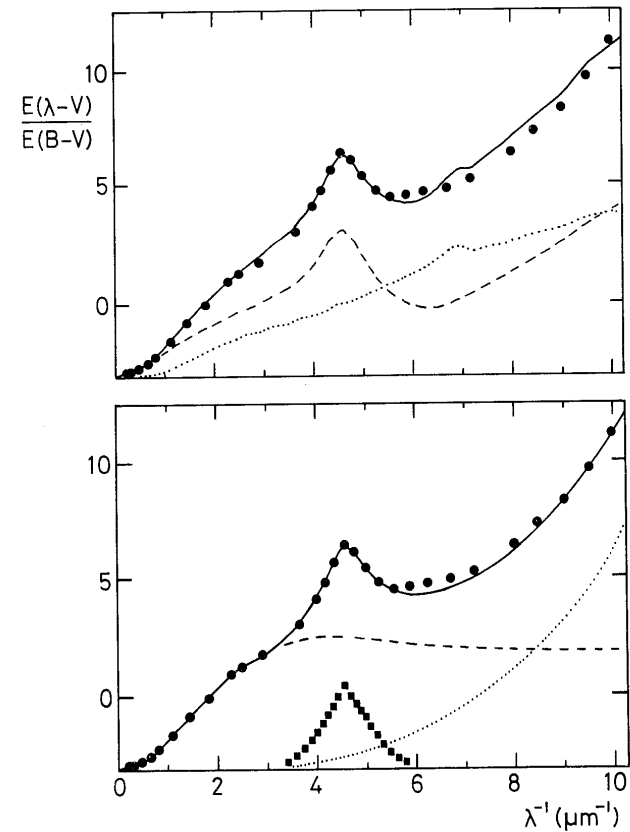
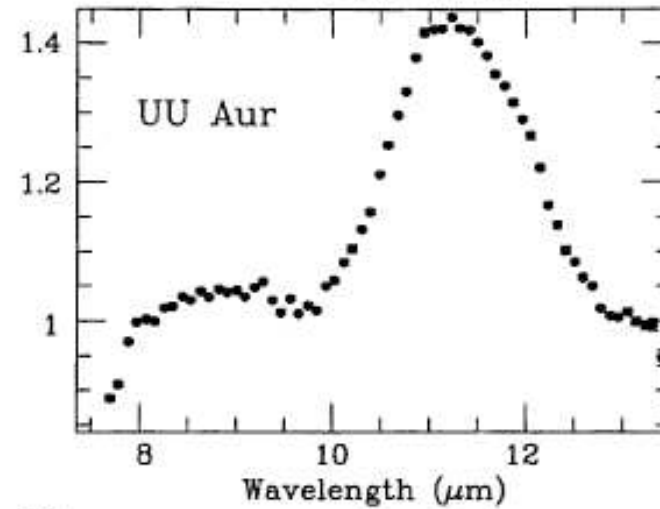
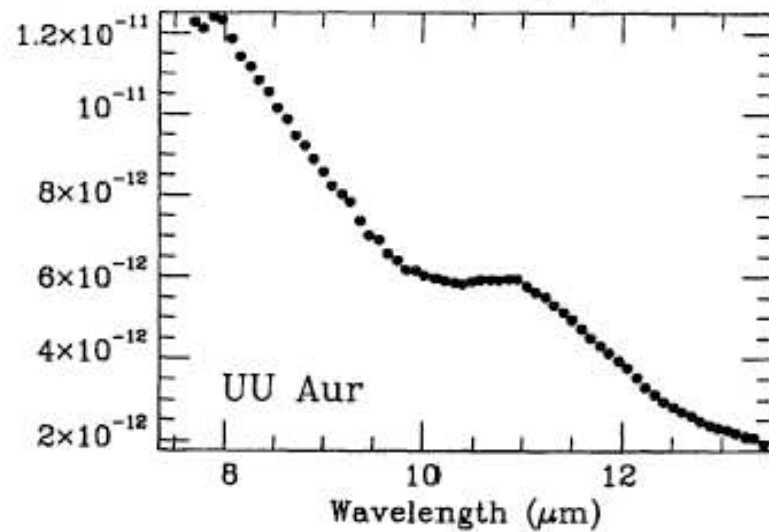


Figure 3.11 Model fits to the observed extinction curve. The mean curve (table 3.1) is plotted as solid circles, as in figure 3.3. Upper frame: the ‘MRN’ two-component model in the version of Draine and Lee (1984), in which graphite (dashed curve) and silicate (dotted curve) contribute to the total extinction (continuous curve). Lower frame: a more general three-component model (e.g. Greenberg 1973), in which ‘classical’ dielectric grains produce wavelength-dependent visual extinction and neutral ultraviolet extinction (dashed curve) and very small grains contribute the far-ultraviolet rise (dotted curve). The  $\lambda_{2175}$  feature is produced by an independent absorbing component (squares).

**SiC** – 11.3  $\mu\text{m}$  seen in emission in some C-rich stellar outflows from stars.



*Spectra of the C-rich star UU Aur. The left spectrum shows the flux data, while the curve on the right has had the background continuum divided out. The 11.3  $\mu\text{m}$  feature is due to SiC.*

**Ices** of  $\text{H}_2\text{O}$ ,  $\text{NH}_3$ ,  $\text{CH}_4$ ,  $\text{CO}$ ,  $\text{CO}_2$  in giant molecular clouds.

These are shown on page 10 of these notes.

## Organics - Polycyclic Aromatic Hydrocarbons (PAHs), Hydrogenated Amorphous Carbon (HACs), etc.

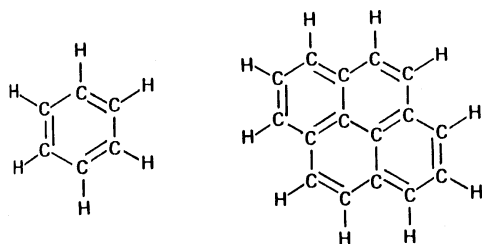


Figure 6.6 The molecular structure of benzene (left) and the 4-ringed polycyclic aromatic hydrocarbon pyrene (right).

Table 6.1 Wavelengths ( $\mu\text{m}$ ) and assignments of the principal spectral features in polycyclic aromatic hydrocarbons (Allamandola *et al* 1989).

$\lambda_{\text{obs}}$	$\lambda_{\text{lab}}$	Assignments
3.29	3.29	C-H stretch ( $\nu = 1 \rightarrow 0$ )
6.2	6.2	C-C stretch
7.7	7.6-8.0	C-C stretch
8.6	8.6-8.8	C-H in-plane bend
11.3	11.2-12.7	C-H out-of-plane bend for peripheral or adjacent H atoms

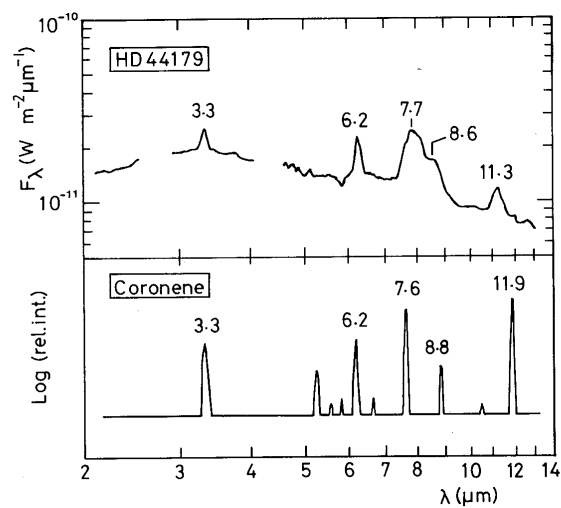


Figure 6.7 The infrared spectrum of HD 44179 in the Red Rectangle (Russell *et al* 1978, upper frame) compared with that for coronene (Léger and Puget 1984). The principal spectral features are labelled by their wavelengths in  $\mu\text{m}$ .

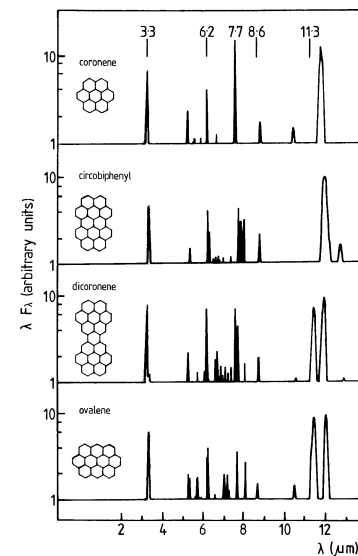
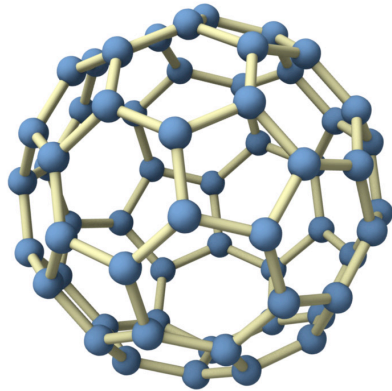
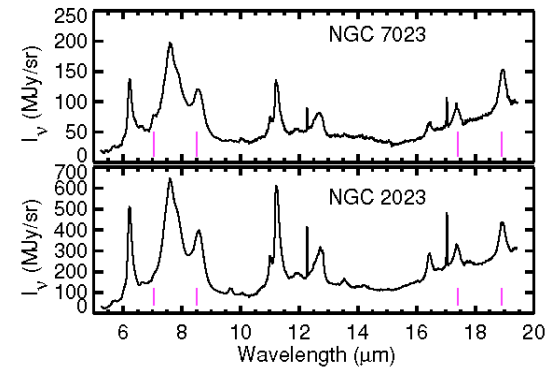


Figure 6.8 Comparison of the predicted emission spectra of several PAHs at 850 K (Léger and d'Hendecourt 1988): from the top, coronene, circobiphenyl, dicoronene and ovalene. The structure of each PAH is shown to the left of the spectrum. The positions of the principal interstellar features are labelled above the upper spectrum.

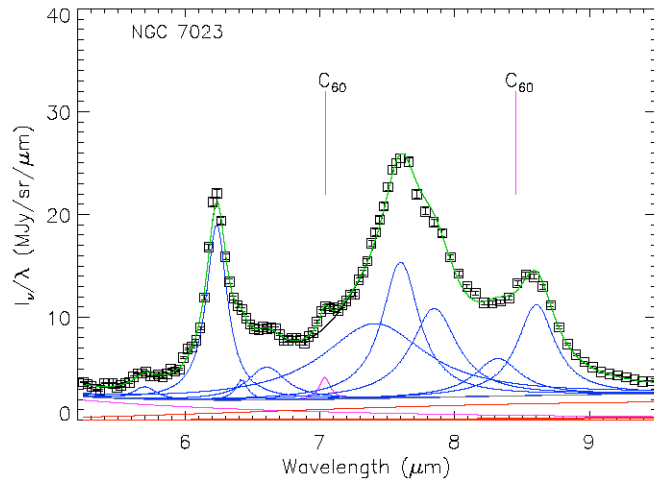
Ensembles of PAHs and C<sub>60</sub> (Buckminsterfullerene – “buckyballs”)



The structure of the C<sub>60</sub> molecule



Locations of C<sub>60</sub> lines in two interstellar sources. From Sellgren et al. 2010, ApJ, 722, L54



The decomposition of the PAH and C<sub>60</sub> components in the spectrum of NGC 7023. From Sellgren et al. 2010, ApJ, 722, L54

Others? Diffuse Interstellar Bands (DIBs) – ionized PAHs?

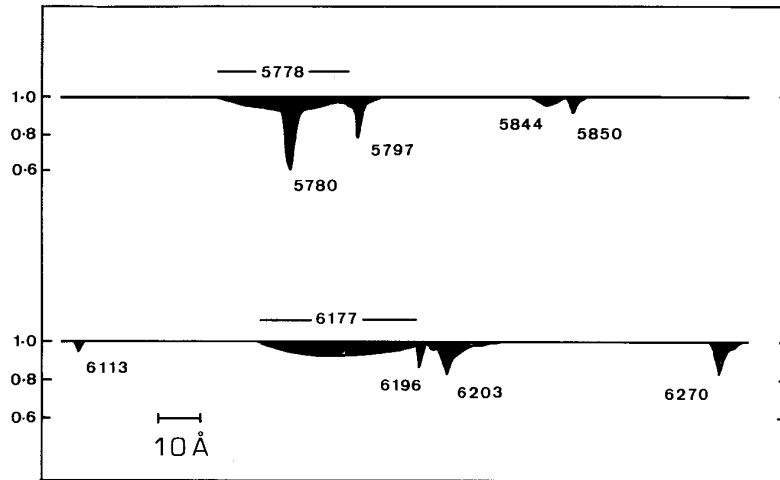


**Figure 5.5** A schematic representation of diffuse bands in the yellow-red region of the spectrum, based on intensity traces for the reddened star HD 183143 (Herbig 1975). Interstellar absorptions are shown in the wavelength range 5730-5900 Å (above) and 6110-6280 Å (below). Photospheric and telluric features in the spectra are eliminated with reference to corresponding data for a comparison star ( $\beta$  Orionis) of similar spectral type and low reddening.

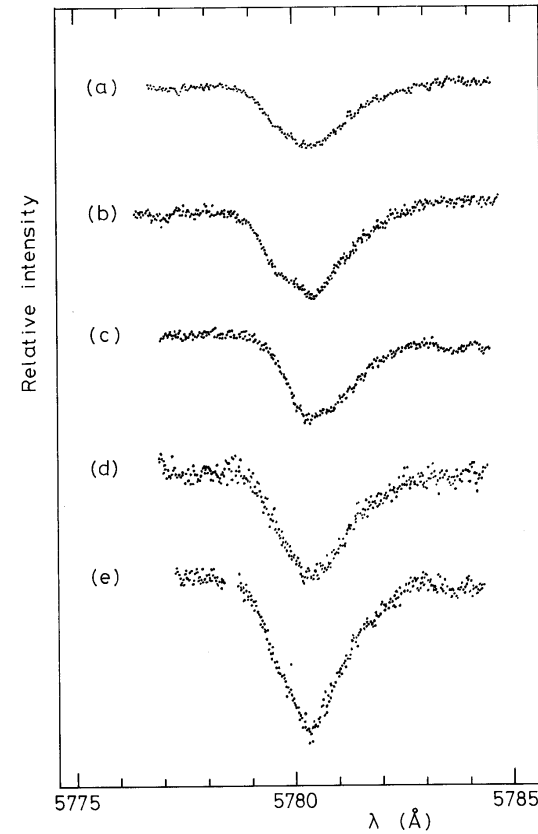
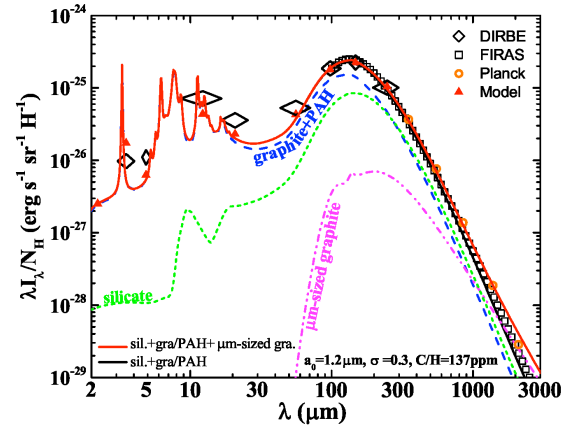
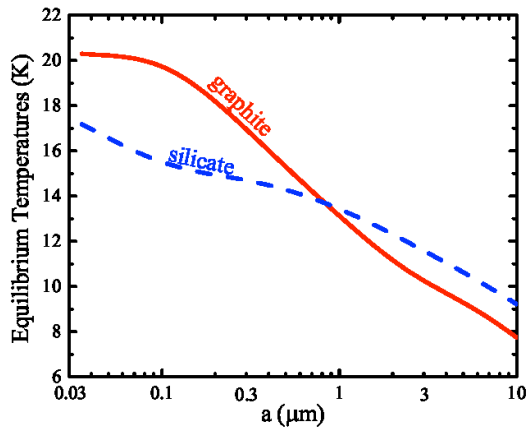
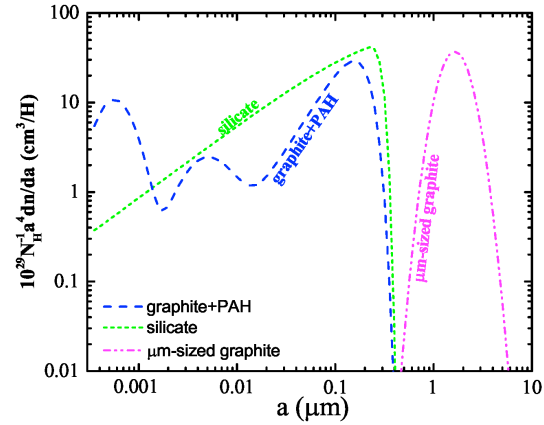
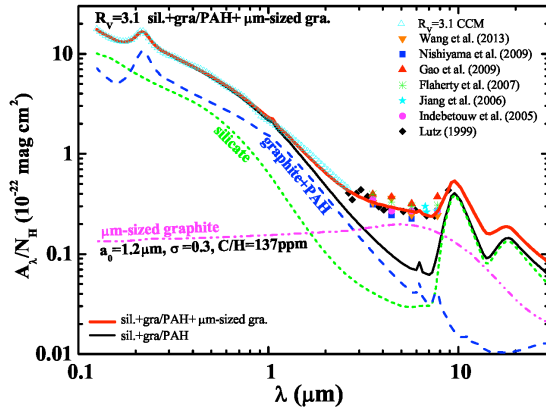


**Figure 5.7** Profiles of the  $\lambda 5780$  diffuse interstellar band at a spectral resolution of 0.07 Å: (a)  $\sigma$  Sco; (b)  $\chi^2$  Ori; (c)  $\nu$  Cep; (d) HD 21389; (e) HD 187982. The central wavelength is standardized to that of  $\sigma$  Sco, on the assumption that differences present in the original spectra are the result of Doppler shifts due to cloud motions. (Adapted from Snell and Vanden Bout 1981.)

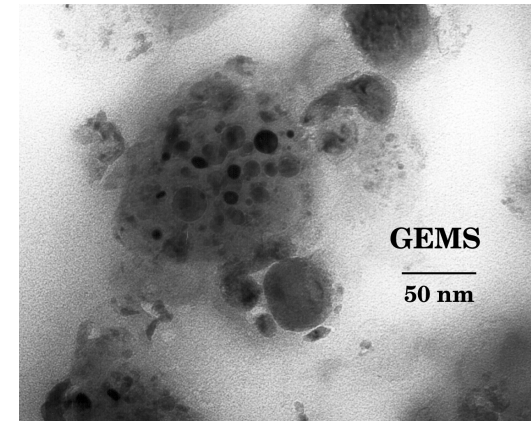
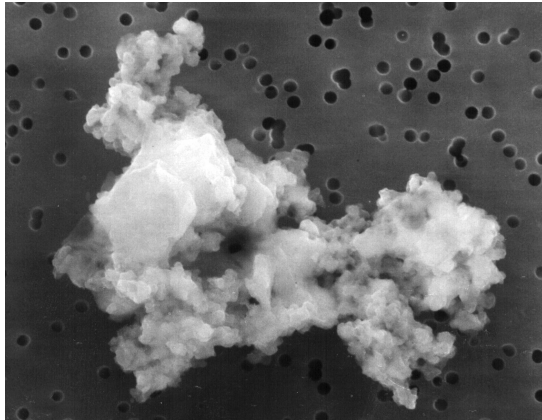
## The Infrared Interstellar Extinction & Emission Curves (Recent Work)

While many studies of the interstellar extinction have suggested that ISM grains are dominated by sub-micron sized grains, the 3-10  $\mu\text{m}$  extinction along many lines of sight may require a different “prescription” that includes grains larger than this – see Wang et al. 2015, arXiv 1508.03403.



## Interstellar Dust in the Laboratory?

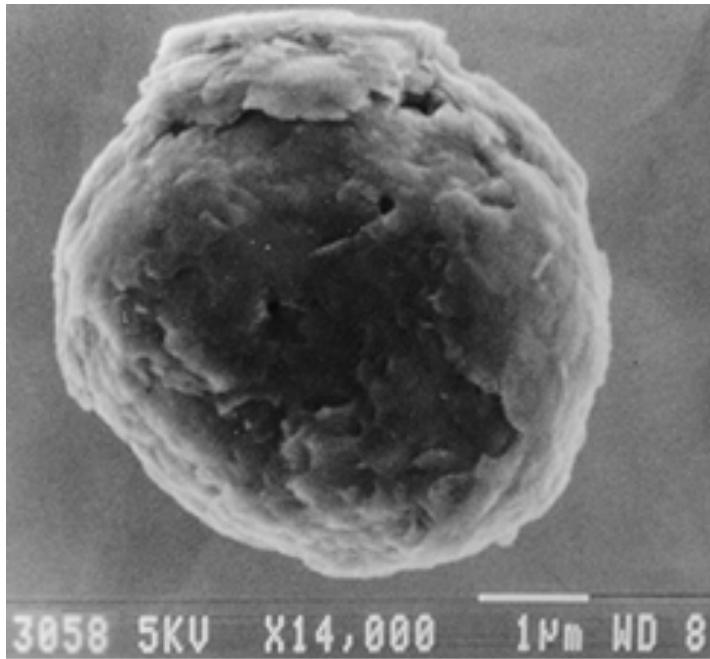
Interstellar dust grains that survived the formation process of our solar system were incorporated in comets in a relatively unprocessed state. These grains can be collected in the Earth's atmosphere and studied in the laboratory.



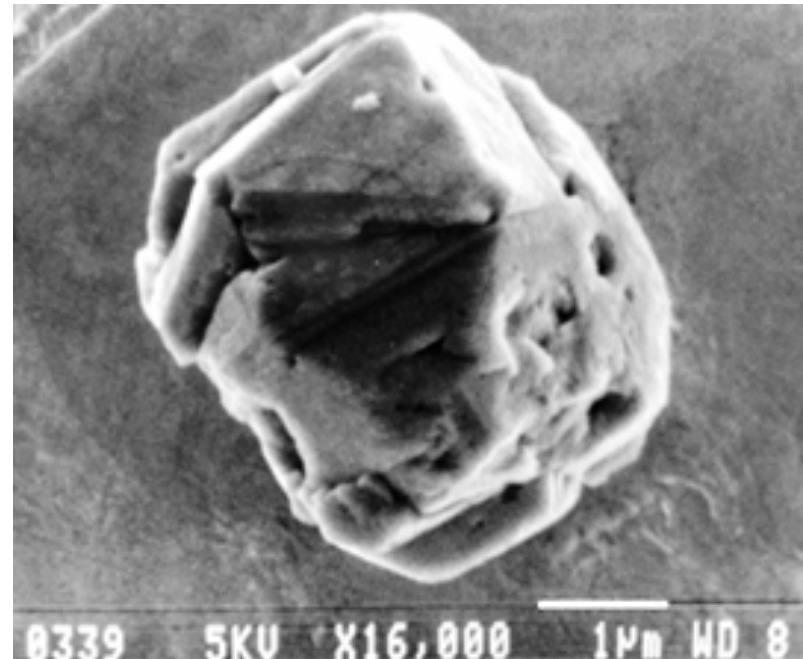
These generally consist of glassy Mg-rich pyroxene (enstatite  $\text{MgSiO}_3$ ) and olivine (forsterite  $\text{Mg}_2\text{SiO}_4$ ) material with a matrix of an organic refractory material. They also contain inclusions of iron that would allow them to become aligned with the galactic magnetic field much more efficiently than was once thought possible for a pure dielectric material (Davis-Greenstein mechanism).

*The physical and chemical structure of the silicate subunits are a heterogeneous mixture of Glass with Embedded Metals and Sulfides = "GEMS".*

Some C-rich meteorites contain graphite and SiC grains that were able to survive the harsh conditions in the inner solar system.



(Scale bar is 1µm.) Photo courtesy of S. Amari.



Scale bar is 1 µm. (Photo courtesy of S. Amari.)

*A graphite "onion" (left) and SiC grain (right) extracted from C-rich meteorites.*



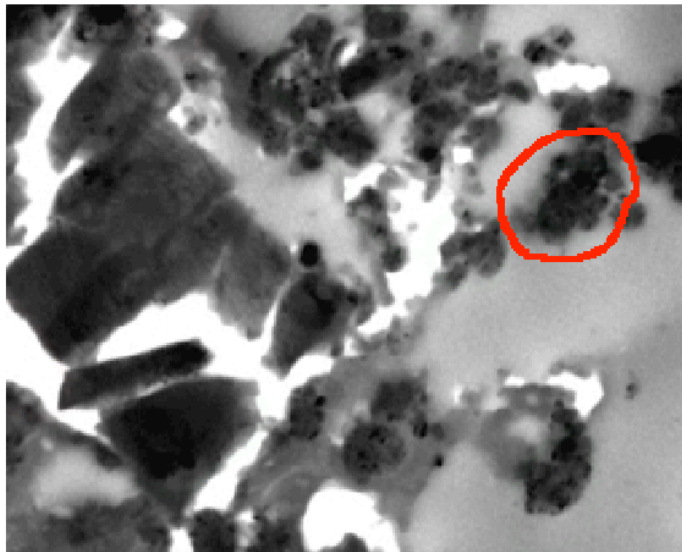


Figure 3: TEM image of L2005C13. The red circle shows the location of a  $^{17}\text{O}$ -rich forsterite grain surrounded by isotopically solar forsterites.

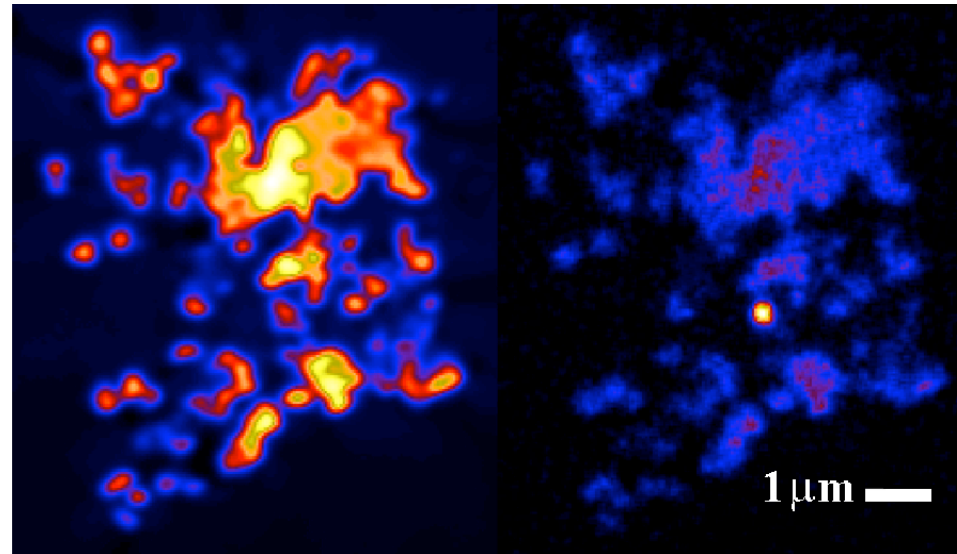
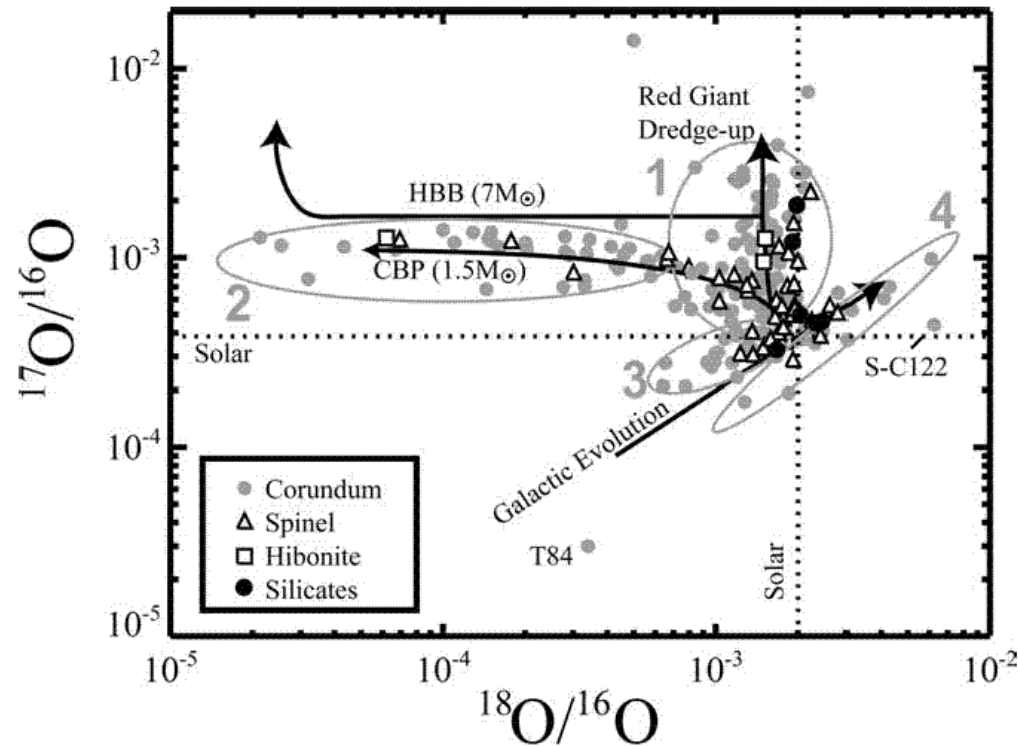


Figure 1:  $^{16}\text{O}$  (left) and  $^{17}\text{O}$  (right) images of IDP L2005C13. The bright region in the  $^{17}\text{O}$  image marks a 0.25  $\mu\text{m}$  presolar silicate grain with  $^{16}\text{O}/^{17}\text{O} \sim 440$  (solar = 2610).

Isotopic anomalies provide clues about the origin of these grains.

Isotopes of O point to an origin at the base of the convection zone in AGB stars, while 3<sup>rd</sup> dredge-up material is rich in <sup>13</sup>C.



**Figure 4** O isotopic ratios measured in presolar oxide stardust (Choi et al. 1998, 1999; Messenger et al. 2003; Nittler 1997; Zimmer et al. 2003b). Gray ellipses indicate grain groups defined by Nittler et al. (1997). Theoretical expectations for Galactic evolution (Timmer et al. 1995), red giant dredge-up (Boothroyd & Sackmann 1999), cool-bottom processing (CBP) (Nollett et al. 2003, Wasserburg et al. 1995), and hot-bottom burning (HBB) (Boothroyd et al. 1995) are schematically shown.